Ultrafast Resonant Interatomic Coulombic Decay Induced by Quantum Fluid Dynamics

A. C. LaForge,[1,2,*] R. Michiels,[2] Y. Ovcharenko,[3,§] A. Ngai,[2] J. M. Escartín,[4] N. Berrah,[1] C. Callegari,[5] A. Clark,[6] M. Coreno,[7] R. Cucini,[5] M. Di Fraia,[5] M. Drabbels,[6] E. Fasshauer,[8] P. Finetti,[5] L. Giannessi,[5,9] C. Grazioli,[18] D. Iablonskyi,[10] B. Langbehn,[3] T. Nishiyama,[11] V. Oliver,[6] P. Piseri,[12] O. Plekan,[5] K. C. Prince,[5] D. Rupp,[3,¶] S. Stranges,[13] K. Ueda,[10] N. Sisourat,[14] J. Eloranta,[15] M. Pi,[16,17] M. Barranco,[16,17] F. Stienkemeier,[2] T. Möller,[3,†] and M. Mudrich[8,‡]

[1]*Department of Physics, University of Connecticut, Storrs, Connecticut 06269, USA*
[2]*Institute of Physics, University of Freiburg, 79104 Freiburg, Germany*
[3]*Institut für Optik und Atomare Physik, Technische Universität Berlin, 10623 Berlin, Germany*
[4]*Institut de Química Teòrica i Computacional, Universitat de Barcelona, Carrer de Martí i Franquès 1, 08028 Barcelona, Spain*
[5]*Elettra-Sincrotrone Trieste, 34149 Basovizza, Trieste, Italy*
[6]*Laboratoire Chimie Physique Moléculaire, Ecole Polytechnique Fédérale de Lausanne, 1015 Lausanne, Switzerland*
[7]*CNR, Istituto di Struttura della Materia, 00016 Monterotondo Scalo, Italy*
[8]*Department of Physics and Astronomy, Aarhus University, 8000 Aarhus C, Denmark*
[9]*Nazionale di Fisica Nucleare, Laboratori Nazionali di Frascati, Via E. Fermi 40, 00044 Frascati, Roma, Italy*
CNR-Istituto Officina dei Materiali, Laboratorio TASC, 34149 Trieste, Italy
[10]*Institute of Multidisciplinary Research for Advanced Materials, Tohoku University, Sendai 980-8577, Japan*
[11]*Division of Physics and Astronomy, Graduate School of Science, Kyoto University, Kyoto 606-8502, Japan*
[12]*Dipartimento di Fisica and CIMaINa, Università degli Studi di Milano, 20133 Milano, Italy*
[13]*Department of Chemistry and Drug Technologies, University Sapienza, 00185 Rome, Italy*
[14]*Sorbonne Université, CNRS, Laboratoire de Chimie Physique Matière et Rayonnement, UMR 7614, F-75005 Paris, France*
[15]*Department of Chemistry and Biochemistry, California State University at Northridge, Northridge, California 91330, USA*
[16]*Departament FQA, Facultat de Física, Universitat de Barcelona, Barcelona, 08028, Spain*
[17]*Institute of Nanoscience and Nanotechnology (IN2UB), Universitat de Barcelona, Barcelona, 08028, Spain*

(Received 3 September 2020; revised 5 January 2021; accepted 19 February 2021; published 12 April 2021)

Interatomic processes play a crucial role in weakly bound complexes exposed to ionizing radiation; therefore, gaining a thorough understanding of their efficiency is of fundamental importance. Here, we directly measure the timescale of interatomic Coulombic decay (ICD) in resonantly excited helium nanodroplets using a high-resolution, tunable, extreme ultraviolet free-electron laser. Over an extensive range of droplet sizes and laser intensities, we discover the decay to be surprisingly fast, with decay times as short as 400 fs, nearly independent of the density of the excited states. Using a combination of time-dependent density functional theory and *ab initio* quantum chemistry calculations, we elucidate the mechanisms of this ultrafast decay process, where pairs of excited helium atoms in one droplet strongly attract each other and form merging void bubbles, which drastically accelerates ICD.

DOI: 10.1103/PhysRevX.11.021011

Subject Areas: Atomic and Molecular Physics, Chemical Physics, Superfluidity

[*]aaron.laforge@uconn.edu
[†]thomas.moeller@physik.tu-berlin.de
[‡]mudrich@phys.au.dk
[§]Present address: European XFEL, 22869 Schenefeld, Germany.
[¶]Present address: Laboratory for Solid State Physics, ETH Zurich, 8093 Zurich, Switzerland.

I. INTRODUCTION

In molecular and condensed-phase systems, interatomic processes offer a means for localized energy or charge to disperse to the surrounding environment. The diversity of these processes often makes it tedious or impossible to obtain a complete picture of the ionization mechanisms and dynamics. Alternatively, free, weakly bound nanosystems, such as van der Waals (vdW) clusters, can be used to study such interatomic interactions in a well-controlled manner. In particular, the study of vdW clusters irradiated by intense extreme ultraviolet (XUV) free-electron laser (FEL) radiation has led to the observation of numerous novel interatomic processes [1–3]. An important type of interatomic process known as interatomic Coulombic decay (ICD) [4] has been widely studied in weakly bound systems [5–7]. In cases where local Auger decay is energetically forbidden, an excited atom or molecule releases its excitation energy by transferring it to a neighboring atom or molecule, which can result in its ionization. In general, ICD is a prominent decay mechanism in a multitude of systems, specifically those of biological relevance [8–11]. A key parameter in determining the importance of ICD in a nanosystem is its decay time, which is directly linked to its efficiency. With the advent of seeded FELs and the availability of intense, tunable XUV radiation [12,13], new types of resonant ICD [14] have been observed in vdW clusters [15–18], where at least two photons are absorbed and energy is exchanged between neighboring excited atoms. More importantly, FELs offer the capability to directly follow the dynamics of ICD in the time domain. So far, ultrafast time-resolved measurements have been limited to ICD in vdW dimers [19,20]. Although vdW dimers, a type of weakly bound molecular system, are of fundamental interest, they can by no means exemplify the complex dynamics occurring in a nanoparticle or condensed-phase system where multiple intermolecular processes can play a critical role.

He nanodroplets serve as model nanosystems in numerous research fields, since they can bridge the gap between simple atomic and molecular systems and extended, condensed-phase systems [21]. Because of their extremely weak interatomic binding, superfluid nature, and simple electronic structure, He nanodroplets are an ideal environment to study interatomic processes in a homogeneous liquid [15,16,18,22,23] or in a well-defined heterocluster, as is the case for doped He nanodroplets [24–29]. When the He environment is excited, a void bubble, or "cavity," is formed around the excited atom [30,31], which can freely move about the droplet. This phenomenon is a general feature in closed-shell systems where the local environment tends to exert a repulsive force on electrons or impurities with a low electron affinity due to the Pauli exclusion principle. This interaction induces the formation of cavities around the impurities and possible clustering or assembly thereof [32]. A similar, although more complicated, process of cavity formation occurs in classical fluids and is responsible for molecular solvation. For example, in water, the so-called hydrophobic effect determines whether a molecule is individually hydrated or assembles into a larger structure [33].

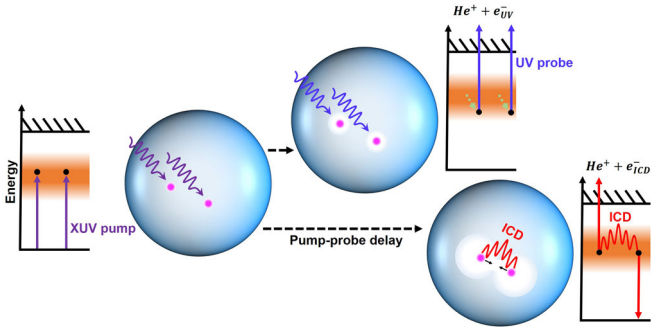

FIG. 1. Atoms in the He droplet are excited to the $1s2p$ droplet band by the XUV pump pulse. After internal relaxation, bubbles are formed around the excited atoms. The two bubbles are accelerated toward each other, leading to a merging of the bubbles and ICD (bottom scenario). A time-delayed UV pulse is used to probe the dynamics of the process. If the UV probe pulse comes before ICD occurs, the pulse ionizes the excited atoms, thereby halting the ICD process (top scenario at short pump-probe delay). The He droplet is represented by the large blue circles, and excited atoms and bubbles are represented by pink and white circles, respectively. The energy-level diagrams illustrate the energetics of processes. Using photoelectron spectroscopy, one can differentiate ICD electrons and UV-ionized electrons as shown in Fig. 2.

Here, we report on time-resolved measurements of resonant ICD in nanoparticles, where He droplets are chosen as a model system. The process is schematically shown in Fig. 1. Atoms are excited by an XUV pulse tuned into resonance with the $1s2p$ droplet band ($h\nu = 21.6$ eV) [34]. The pulse creates multiple excited atoms in the droplet which can decay via ICD; i.e., the energy from one excited He atom, He^*, is transferred to another He^*, which, in turn, is ionized. A second, time-delayed UV pulse can directly ionize the excited atom(s) in the droplet, thereby interrupting and halting any interatomic decay processes. Over an extensive range of droplet sizes and laser pulse energies, the decay mechanism is found to be much faster than predicted by theory [14]. Even more surprisingly, the decay rate is nearly independent of the number of excited atoms per droplet, although theory predicts a very strong dependence on the internuclear distance [14]. To understand these discrepancies, the experimental results are modeled using a combination of time-dependent density-functional theory (TDDFT) [35,36] and *ab initio* calculations of the doubly excited He^*-He^* pair potentials as well as the ICD widths.

We discover that the ICD dynamics are largely determined by the attractive interaction of closely spaced He^* atoms and by the formation of bubbles around them. The latter strongly accelerates the ICD via the merging of overlapping bubbles. Previous experimental work on bubble formation in He droplets [31] focuses on the relaxation

of one excitation in a droplet, which forms a single bubble in the course of its relaxation. In contrast, here, the focus is on ultrafast dynamics between two bubbles, which facilitates the ICD process. Overall, the relevance of our findings is (i) realizing that, in a condensed-phase system, ICD is not only determined by the electronic interaction of the two atoms involved, but it can be crucially influenced by the response of the surrounding medium, and (ii) the resulting ICD time is drastically reduced to the femtosecond range, in contrast with previous expectations that this type of ICD is much slower, i.e., tens to hundreds of picoseconds [14,17].

II. EXPERIMENT

This work is performed at the low density matter end station [37] of the seeded FEL FERMI, in Trieste, Italy. The FEL photon energy (21.6 eV) is tuned via the seed laser, undulator gaps, and other machine parameters, yielding a pulse length of approximately 100 fs full width at half maximum (FWHM) [12,13]. The measurements are taken over two separate periods with different experimental conditions. The second set of parameters is given in parentheses. The FEL pulse energy, varied from 0.1 to 50 μJ, is determined upstream by gas ionization, taking the nominal reflectivity of the optical elements in the beam transport system into account. The diameter of the FEL focus is 250 μm FWHM. The UV probe pulse is obtained from a frequency-tripled (-doubled) Ti:sapphire laser [$h\nu' = 4.8$ (3.2) eV] with a pulse energy of 50 (200) μJ and a focus diameter of 250 μm FWHM. A tin filter of 160 nm thickness is used to suppress higher-order harmonic radiation. The cross-correlation between the FEL and the probe laser is 200 fs FWHM, measured by resonant two-photon ionization of He gas. A supersonic jet of He nanodroplets is produced by expansion of high-pressure He gas through a pulsed, cryogenically cooled Even-Lavie nozzle. By varying the expansion conditions (backing pressure and nozzle temperature), the mean cluster size is varied in the range of $\langle N \rangle = 10^2$–10^5 He atoms [38]. The nanodroplet beam is perpendicularly crossed by the FEL and UV beams at the center of a velocity map imaging spectrometer [37]. The electron kinetic energy distributions are reconstructed using the maximum entropy velocity Legendre reconstruction method [39].

III. RESULTS AND DISCUSSION

Figure 2(a) shows the distributions of electron kinetic energy E_e emitted by resonantly excited He droplets as a function of the delay between XUV pump and UV probe laser pulses. The mean droplet size is $\langle N \rangle = 76\,000$ atoms, and the XUV intensity is 2.8×10^9 W/cm^2. At low kinetic energies ($0 < E_e < 2$ eV), the electron distribution is created by resonant two-photon ionization (2PI) in He nanodroplets. At short delays, $\Delta t < 1$ ps, the distribution shows the droplet-induced relaxation dynamics of He* from the XUV-excited $1s2p$ state to the $1s2s$ state [31]. At higher kinetic energies ($15 < E_e < 18$ eV), resonant multiphoton ICD is observed according to the reaction [14–16,18]

$$(\mathrm{He}^* + \mathrm{He}^*)\mathrm{He}_{N-2} \rightarrow (\mathrm{He}^+ + e_{\mathrm{ICD}} + \mathrm{He})\mathrm{He}_{N-2}.$$

Here, He_{N-2} denotes the He droplet, and e_{ICD} is the ICD electron. A discussion of the electronic states which initiate this type of ICD is given in the Appendix A. Since resonant ICD is a binary process, at least two excited atoms are required per droplet.

The intensities of photoelectrons (red squares) and ICD electrons (blue circles), depicted in Fig. 2(b), display opposing trends in their time evolution: The 2PI signal

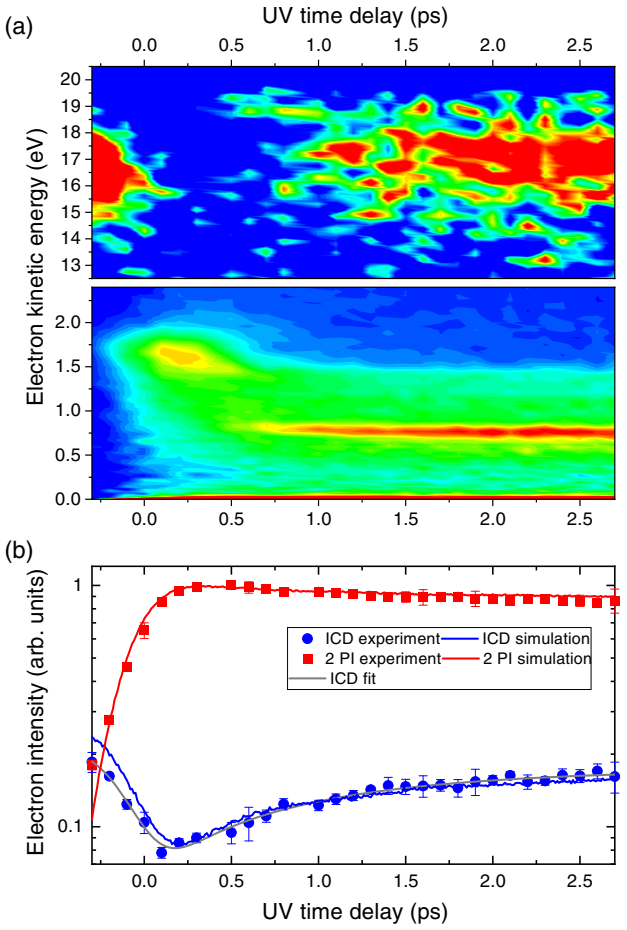

FIG. 2. (a) Time-resolved electron kinetic energy distributions of resonantly excited He droplets centered around the ICD peak (top) and the two-photon ionization (2PI) signal (bottom). (b) Projection of the intensity of the ICD peak (blue circles) and the 2PI signal (red squares) as a function of XUV-UV pump-probe delay. The experimental data are fitted with an exponential decay function convoluted with a cross correlation function (gray line). The red and blue lines show the results of a MC simulation (see the text for details). The droplet size is 76 000 atoms, and the excitation photon energy is 21.6 eV.

is enhanced at delays $0 < \Delta t < 0.2$ ps, whereas the ICD signal is depressed. This result can be rationalized by the depletion of the He^* population through photoionization by the UV probe pulse, thereby suppressing the ICD. As the pump-probe delay is increased, ICD can proceed before the He^* are photoionized and the e_{ICD} yield is replenished. Thus, the rise of the e_{ICD} yield reflects the timescale of the ICD. To quantify this process, the ICD signal is fitted with a function [gray line in Fig. 2(b)] accounting for the exponential rise as well as the pump-probe cross correlation. A thorough discussion of the fitting procedure is given in Appendix B. Figure 2(b) also shows the ICD (blue line) and 2PI (red line) data from a Monte Carlo (MC) simulation as discussed later in the text. Additional data and fits for different experimental parameters are given in Appendix C.

To systematically investigate the dynamics of ICD in He nanodroplets, pump-probe delay dependences over a wide range of He droplet sizes and XUV intensities are recorded. The latter controls the He^* excitation probability (photon flux × absorption cross section) and thereby the mean distance between He^* in a droplet. Because of the strong coupling between the FEL power, droplet size, and collective autoionization (CAI) effects [18], only a limited range of excitation probabilities (0.1%–1%) show a clearly distinguishable ICD peak, despite the broad range of droplet sizes and FEL intensities available. As the FEL intensity increases, multiple excited atoms may interact, leading to decay by CAI and formation of a nanoplasma [16]. In the transition from ICD to CAI, the ICD peak broadens and shifts to lower energies due to the formation of a collective Coulomb potential and eventually becomes dominated by low-energy thermal electrons from the nanoplasma [18].

Similar to what is shown in Fig. 2(b), each ICD delay dependence is fitted with a function to determine the time constant of the e_{ICD} evolution. The resulting ICD times τ_{ICD} and e_{ICD} yields are, respectively, plotted as red symbols in Figs. 3(a) and 3(b) as a function of the excitation probability. The corresponding MC simulation results are shown as blue dots. The e_{ICD} yield is determined from the total number of detected electrons and the He^* photoionization cross section [40]. It is normalized to the number of He^* atoms in the droplet and multiplied by 2 to account for the fact that two excitations produce one ICD electron. The resulting ICD efficiency rises from 0.09 to 0.32 in the given range of He^* excitation probability, while τ_{ICD} decreases from 1000 to 400 fs. To decouple the effect of the droplet size from the FEL intensity, we additionally perform MC simulations (see Supplemental Material [41] for details) for fixed droplet sizes. The results for small and large droplets are shown in Fig. 3 as black and gray lines, respectively. For small droplets, the ICD time is nearly constant and lower than the ICD decay times for large droplets, which show a weak dependence on the FEL intensity. The ICD efficiency shown in Fig. 3(b) rises from zero as a function

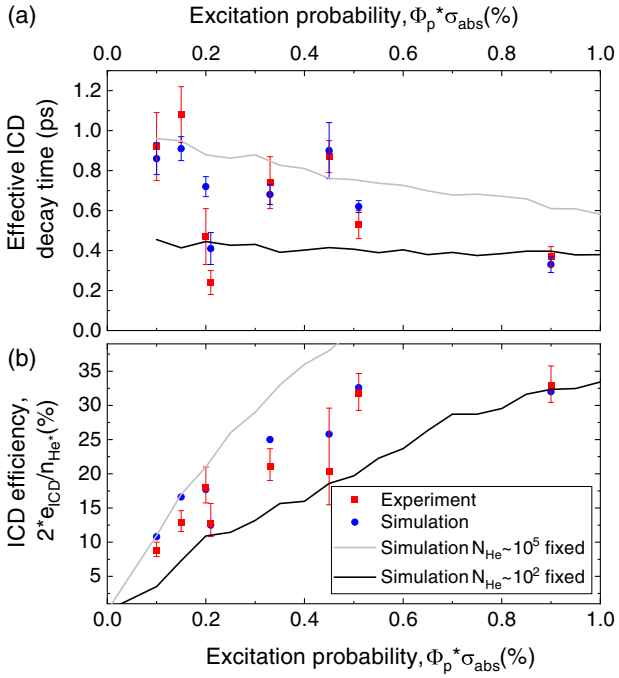

FIG. 3. (a) Effective ICD decay time and (b) ICD efficiency plotted as a function of the excitation probability (red squares). MC simulation results for the specific experimental conditions, droplet size, and FEL intensity are shown as blue dots. Additionally, to show the general trend in the simulations on the FEL intensity, the results for fixed small and large droplets are shown as black and gray lines, respectively.

of the excitation probability with a higher slope for large droplets. Overall, the MC simulations are in excellent agreement with the experimental data.

In general, the measured ICD decay times are surprisingly short ($\tau_{ICD} < 1$ ps) compared to estimates based on the virtual photon ICD model for this type of decay, which yield 52 ps for the fastest channel [14]. Furthermore, previous static measurements predict this type of ICD to be much slower, in the high picosecond range [17,28]. Further proof of the discrepancy between theory and experimental results can be seen in Fig. 4(c), which shows the ICD decay width Γ as a function of the He^*-He^* distance. $\Gamma(d)$ is calculated by the Fano-CI-Stieltjes method [42] for all possible combinations of electronic states populated during droplet relaxation [28,31] (see Supplemental Material [41] for details). Γ, which is inversely proportional to the decay time τ_{ICD}, shows a very strong dependence on the He^*-He^* distance. On the other hand, the measured τ_{ICD}, in Fig. 3(a), shows only a weak dependence on the He^* excitation probability, which is a measurable quantity proportional to the mean He^*-He^* distance. The observed ultrafast ICD rates, in the femtosecond regime, can be explained only through an additional mechanism that brings the two He^* atoms into close contact. Excitation migration [43,44], excitation

delocalization [45], and hole hopping have been discussed extensively over the years, especially in the context of Penning ionization [44,46]. While fast excitation transfer, akin to exciton hopping, can explain the high efficiency of the Penning process [44], it cannot account for the short ICD lifetime. Delocalization of excitations over an extended region of the He droplet as a consequence of exciton hopping would lead to a reduced local spatial overlap and, thus, to low ICD rates. Besides, the large variation of the interatomic distances between He atoms in the droplets due to the large zero-point motion as well as many-body quantum effects may also limit delocalization [45,46]. Unfortunately, the problem of excitation transfer in superfluid He has not yet been addressed theoretically, despite the numerous experimental Penning ionization studies. That said, an additional mechanism is required that brings two He^* into close contact such that ICD takes place at short distances.

Aside from the fast delay-time dependence of the ICD signal, we observe that the e_{ICD} yield in most cases does not fully rise to the level measured at negative delays within the full range of pump-probe delays; see Appendixes B and C. This result indicates that some of the He^* decay by ICD much more slowly than the experimentally observed asymptotic value from which we deduce τ_{ICD}. Furthermore, the observation that the ICD efficiency never exceeds 35% in our experiments points at a competing relaxation channel that prevents the majority of He^* from decaying via ICD.

To better understand the response of He nanodroplets to multiple excitations and to rationalize our experimental findings, TDDFT simulations are performed [31,35,36,47] for the motion of He^* pairs. To keep the simulations tractable, we consider bulk superfluid He, which is coupled to the He^* pair self-consistently. Because of the light mass of the He^* "impurities," they must be treated quantum mechanically with the potential term given by the He^*-droplet interaction. To include the interaction between the two He^* atoms, the He^*-He^* pair potentials are calculated using highly correlated *ab initio* methods (see Supplemental Material [41] for details).

Figure 4(a) shows the time evolution of the 2D cuts of the He density distribution (yellow-red area) when the two excited He atoms are initially separated by $d_0 = 10$ Å (pink-green dots). Animations of these simulated dynamics for various initial conditions are included in Supplemental Material [41]. Upon excitation, bubbles form around them due to the repulsion between the Rydberg electrons and the surrounding closed-shell He atoms [30,31,47–49]. As the bubbles grow and the two He^* atoms weakly attract each other, the bubbles eventually overlap and merge into one large bubble. The salient feature is that, shortly after the two bubbles coalesce, the two He^* are strongly accelerated toward each other. This process is facilitated by the merging

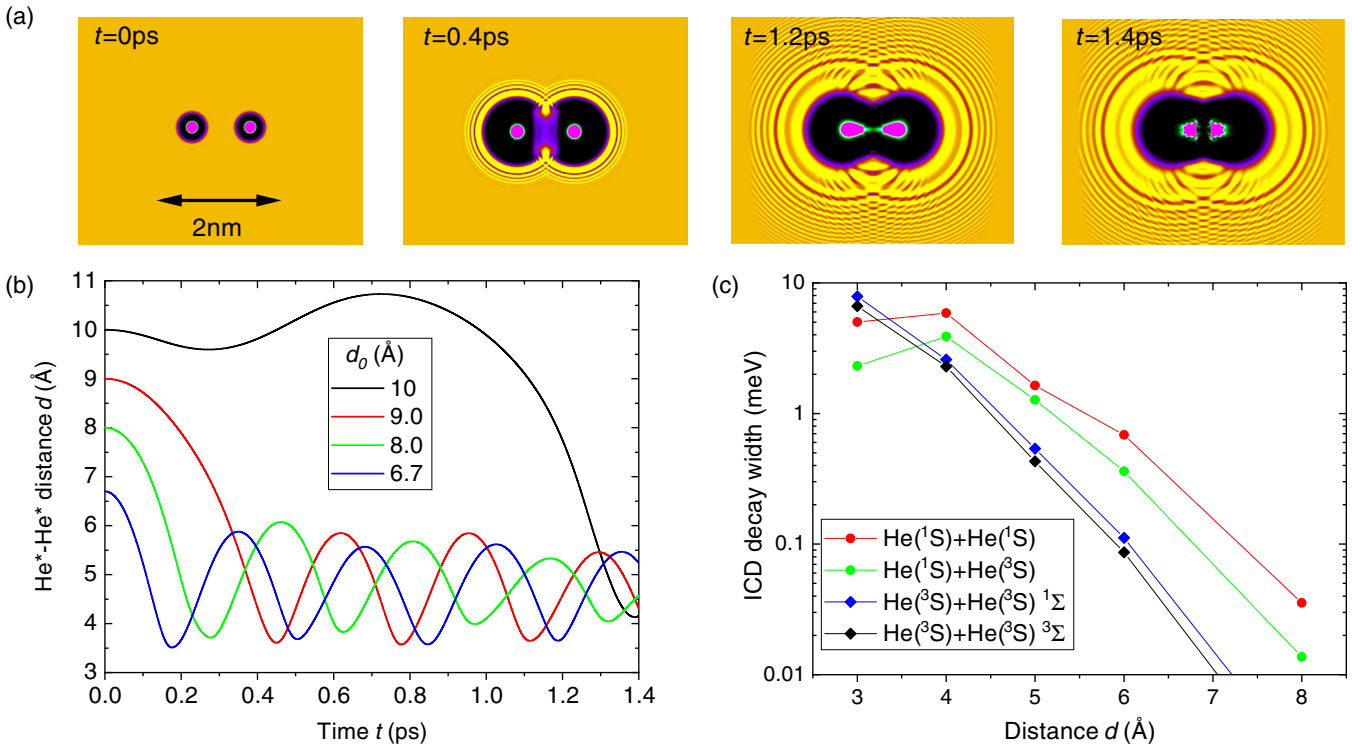

FIG. 4. (a) Snapshots of the He density evolution around two He^* centers separated initially by $d_0 = 10$ Å. The probability distribution of He^* is represented as pink dots, and the black areas show the void bubbles forming. (b) Evolution of the He^*-He^* distance d for various values of the initial distance d_0. (c) Calculated ICD widths for various combinations of $1s2s$-excited He^* atomic states.

of the bubbles where the He^* reach interatomic distances $d < 4$ Å within 400 fs for all initial distances d_0 up to 9 Å; see Fig. 4(b). As ICD is not explicitly included in the TDDFT simulations, the He^* pair continues vibrating at a short distance due to the attractive He^*-He^* potential. However, within the first half cycle of the vibration, the ICD decay width reaches $\Gamma(d = 4\ \text{Å}) = 5.9$ meV, corresponding to a characteristic ICD time $\tau_{\text{ICD}}^{\text{theo}} = 110$ fs for the $He^*(^1S) + He^*(^1S)$ pair, which has the largest branching ratio in the droplet relaxation [28,31]. Thus, all He^* pairs with $d_0 \lesssim 10$ Å actually decay via ICD within $t \lesssim 1.4$ ps with a probability of near unity. Thus, we conclude that the decay in this particular system is largely determined by the quantum fluid dynamics of the merging bubbles, as well as the pairwise attraction of excited atoms.

For larger initial distances ($d_0 > 10$ Å), the time between He^* excitation and bubble merging quickly increases to $t > 10$ ps, and, therefore, ICD becomes very slow. This result explains the observed incomplete replenishment of the e_{ICD} signal at long pump-probe delays. The question remains why not all He^* decay by ICD, in the absence of the probe pulse. It is known that radiative decay is not expected to play a significant role, since the lifetime is in the nanosecond range [30,50]. Previous experimental and theoretical studies show that, following the bubble formation, some of the He^* remain weakly bound to the He droplet surface, where they eventually form He_2^* excimers [51], whereas others are directly ejected from the droplets [31,48,52]. Once a He^* detaches from the droplet, it can no longer decay via ICD, but it still contributes to the photoionization signal. Based on our measurements [Fig. 3(b)], the fraction of ejected He^* is estimated to be larger than 50%. The competition between direct ejection and ICD for initial distances $d_0 > 10$ Å is strongly dependent on the droplet size.

The ICD dynamics in He nanodroplets are largely governed by the motion of He^* driven by the bubble dynamics and the interatomic He^*-He^* potential, competing against the ejection of surface He^* from the droplet. To account for the aforementioned effects, a simplified MC simulation based on $\Gamma(d)$ is developed. The results are displayed in Fig. 3(b). The He droplet is treated as a homogeneously packed sphere of He atoms represented by equally sized spheres. An initial number of He^*, according to the XUV intensity and the He droplet absorption cross section [34], are placed at random positions within the droplet. Then, for each He^*, the following conditions are tested. If the distance to the droplet surface $d_S < 7.5$ Å and the distance to the nearest-neighbor He^* $d_0 > 9.5$ Å, then the He^* is ejected. If $d_S > 7.5$ Å and $d_0 < 15.5$ Å, then the He^* undergoes ICD; the ICD probability is then calculated based on $\Gamma(d)$ according to the trajectory $d(t)$ obtained from the TDDFT simulations. If $d_S > 7.5$ Å and $d_0 > 15.5$ Å, the He^* does not decay by ICD and only photoionization is possible. The probe pulse is implemented by converting the He^* into photoelectrons at a rate consistent with the experimental estimate. The values $d_0 = 15.5$ Å and $d_S = 7.5$ Å, used as criteria for ICD enhanced by bubble merging and He^* ejection, respectively, are deduced from the TDDFT simulations. Additionally, when the same simulation is performed for fixed positions of He^*, the ICD time constants are 1–2 orders of magnitude longer than the experimental values, thus demonstrating the importance of ultrafast bubble dynamics and the attractive He^*-He^* potential. An in-depth discussion of these simulations is given in Appendix D.

Overall, the conceptual leap presented in our results show that resonant ICD in a superfluid nanosystem is predominantly driven by the ultrafast dynamics of the medium surrounding the interaction centers ($He^* + He^*$, in this case). Previous work on (nonresonant) ICD considers only the dynamics of the interaction centers, not their environment. While this assumption is valid for small systems like dimers and crystalline clusters, in extended condensed-phase systems such as liquids and superfluids, the response of the local environment has to be taken into account. Our work directly demonstrates that the mesoscopic dynamics may drastically enhance the ICD rate. This result has implications for biological systems where the local aqueous medium surrounding the biomolecules may crucially impact the decay rate when being subjected to radiation damage by ICD [10,11].

IV. CONCLUSIONS

In summary, we have performed time-resolved measurements of resonant ICD in He nanodroplets. Over a wide range of droplet sizes and laser pulse energies, we have found the decay to be as fast as 400 fs and to have little dependence on the density of excited states, in contrast to the strong dependence of the predicted ICD decay width on the distance between excitations. Our simulations have shown that the ICD dynamics are largely determined by the pairwise attraction of excited atoms, as well as the peculiar response of He droplets to multiple resonant excitations. The formation of bubbles around the excitations and their subsequent merging accelerates ICD, whereas the ejection of excited state atoms from the droplet competes with it. Thus, using He droplets as a model system bridging molecular and condensed-phase sciences, we have demonstrated that resonant ICD in the condensed phase is governed by ultrafast relaxation mechanisms that couple electronic and nanofluid translational degrees of freedom. These results pave the way for time-resolved measurements of more complex intermolecular decay processes involving He excited state dynamics in doped He droplets, such as ICD-mediated single or double ionization of molecules and clusters [26–28].

Although He nanodroplets are a unique type of quantum fluid, our findings of the bubble dynamics could have

implications for other classical fluid systems where charge, excitations, or impurities can freely move throughout the medium. The dynamics of bubbles, also known as cavities in water, are responsible for a wide variety of fundamental processes, such as protein assembly into functional complexes in biological systems [33] or the behavior of impurities in metals, relevant to materials science [32]. Although classical fluids are more complex than He nanodroplets, intermolecular electronic decay and bubble dynamics are highly relevant processes in these systems. The range of intermolecular decay mechanisms extends beyond ICD [11] to processes such as electron transfer mediated decay [53], exciton-exciton annihilation [54], singlet fission [55], and Förster resonance energy transfer [56]. The rates of these decay mechanisms could be enhanced through bubble dynamics. In this regard, future time-resolved studies where the electronic decay and bubble dynamics could be controlled by laser excitation are of broad interest.

ACKNOWLEDGMENTS

The authors gratefully acknowledge financial support from the Carl-Zeiss-Stiftung, the Deutsche Forschungsgemeinschaft (DFG) under Grant No. MO 719/14-2, within the frame of the Priority Program 1840 "Quantum Dynamics in Tailored Intense Fields" (MU 2347/12-1 and STI 125/22-2), and the Carlsberg Foundation. TDDFT work has been performed under Grant No. FIS2017-87801-P (AEI/FEDER, UE) (M. B. and M. P.). A. C. L. and N. B. acknowledge the support of the Chemical Sciences, Geosciences and Biosciences Division, Office of Basic Energy Sciences, Office of Science, U.S. Department of Energy, Grant No. DE-SC0012376. D. R. acknowledges funding from Leibniz Grant No. SAW/2017/MBI4 and NCCR MUST of the Swiss National Science Foundation (SNF). J. E. acknowledges support from the National Science Foundation Grant No. DMR-1828019. J. M. E. acknowledges support from Ministerio de Ciencia e Innovación of Spain through the Unidades de Excelencia "María de Maeztu" Grant No. MDM-2017-0767.

APPENDIX A: HIGH-RESOLUTION ICD ELECTRON KINETIC ENERGY DISTRIBUTION

Information about the electronic states involved in the ICD process is encoded in the kinetic energy distribution of ICD electrons. Figure 5 shows a high-resolution electron spectrum measured at the photon energy $h\nu = 23.7$ eV. At this photon energy, the $1s4p$ excited state of He droplets is resonantly excited [34]. The mean droplet size is set to 5×10^5 He atoms. Besides the large signal component at low kinetic energy resulting from CAI [16], an additional peak is observed around 16 eV with a shoulder near 15 eV, which is due to ICD. For comparison, we add vertical lines showing the expected ICD electron energies, $E_{e,\mathrm{ICD}}$, for

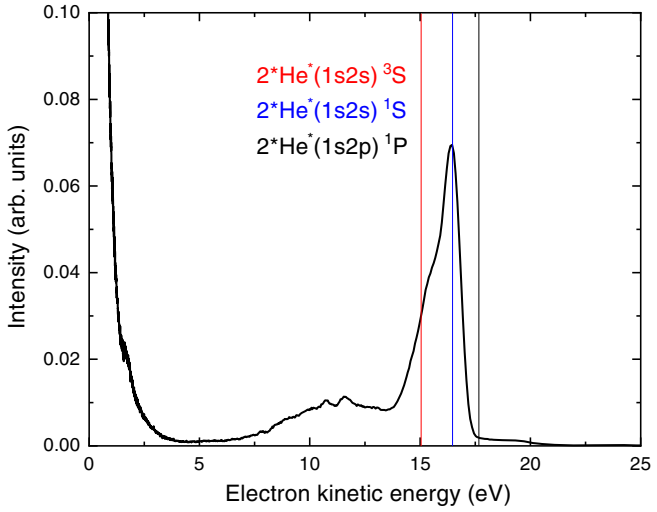

FIG. 5. Static (XUV only) electron kinetic energy distribution measured at $h\nu = 23.7$ eV. The vertical lines depict the nominal values of ICD electron energies for pairs of He* atoms in the three lowest excited states.

pairs of He* in the lowest excited states $2s2s\ ^{1,3}S$ and $2s2p\ ^1P$ according to

$$E_{e,\mathrm{ICD}} = 2E_{\mathrm{He}(1s2s,p)} - E_{i,\mathrm{He}}. \tag{A1}$$

Here, $E_{\mathrm{He}(1s2s,p)}$ is the energy of the $1s2s$, p states of the He atom, and $E_{i,\mathrm{He}}$ is the He ionization potential. Clearly, the $1s2s\ ^1S$ state is the dominant state producing ICD electrons. The $1s2s\ ^3S$ state and He_2^* excimer states (broad feature around $E_{e,\mathrm{ICD}} = 11$ eV) also contribute but to a lesser extent. Although this electron spectrum is measured at a different excitation energy than those in the main text, ICD electrons appear to originate mostly from the same He* states. This result is due to fast electronic relaxation, as previously observed in experiments using high-harmonic laser radiation [57], FEL [18,31], and synchrotron radiation [24,28].

APPENDIX B: FITTING OF ICD ELECTRON YIELDS

The time-dependent ICD electron intensities are fitted with a convolution of the pump-probe cross correlation function obtained by resonant two-photon ionization of He gas and an exponential decay leading to the following function:

$$I(t) = I_0 - A\,\mathrm{erfc}\{[\sigma^2 - \tau(t-t_0)]/(\sqrt{2}\sigma\tau)\} \times \exp[-(t-t_0)/\tau] - B\,\mathrm{erfc}[(t-t_0)/(\sqrt{2}\sigma)]. \tag{B1}$$

This model is the simplest analytic function that reproduces the experimental measurements and is consistent with a more rigorous model of the pump-probe dynamics of ICD processes [58]. The exponential function describes the rise

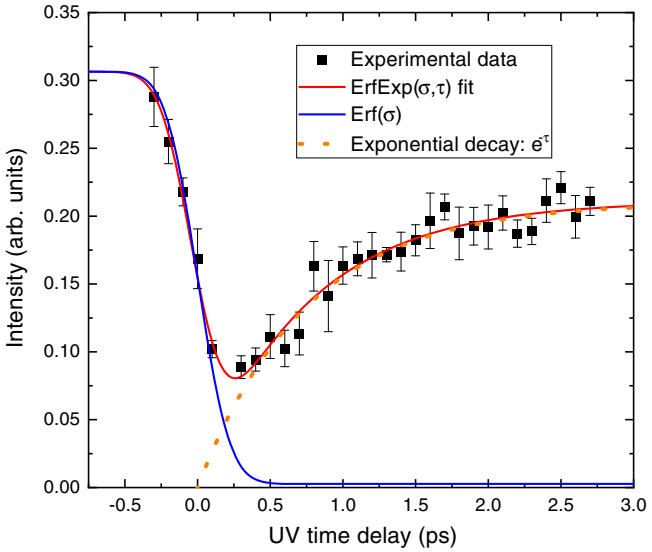

FIG. 6. Fitting of experimental time-resolved ICD data (black squares) with the function from Eq. (B1) (red curve). The components of the fit are illustrated separately: error function (blue curve) and exponential decay (orange dotted line).

of the electron counts for long delay times. Thus, the exponential decay constant τ represents the effective ICD time. The parameter σ represents the cross-correlation width of the two overlapping laser pulses and is fixed to the value measured by resonant two-photon ionization of He gas. The time-zero value t_0 is constrained to 0 ± 15 fs in order to account for possible drifts in the FEL timing. The free parameters I_0, A, and B reflect the total ICD intensity for $t \to -\infty$, $t \to \infty$, and the maximum depletion $I_{\min}$.

Figure 6 displays a fit of a typical experimental measurement. In addition to the full fit curve (red), we show the separate contributions from the error function (blue line) and exponential decay (orange dots).

APPENDIX C: ADDITIONAL EXPERIMENTAL DATA

To give a better overview of the experimental results and systematics, in Fig. 7(a), we show additional pump-probe ICD electron yields measured under different experimental conditions. The red symbols correspond to small droplets with high excitation density. The resulting ICD curve is characterized by a fast time variation, as the mean interatomic distance between excited atoms is small, $d < 10$ Å, and, thus, ICD is fast. The black curve is for an intermediate excitation density and intermediate droplet sizes. The blue curve is for large droplets combined with a low excitation density. Replenishment of the ICD electron signal after depletion is slower, as ICD mostly occurs for pairs of He^* with larger initial separation. Figure 7(b) shows the results of the MC simulation for the same parameters as in the experiment. The good agreement

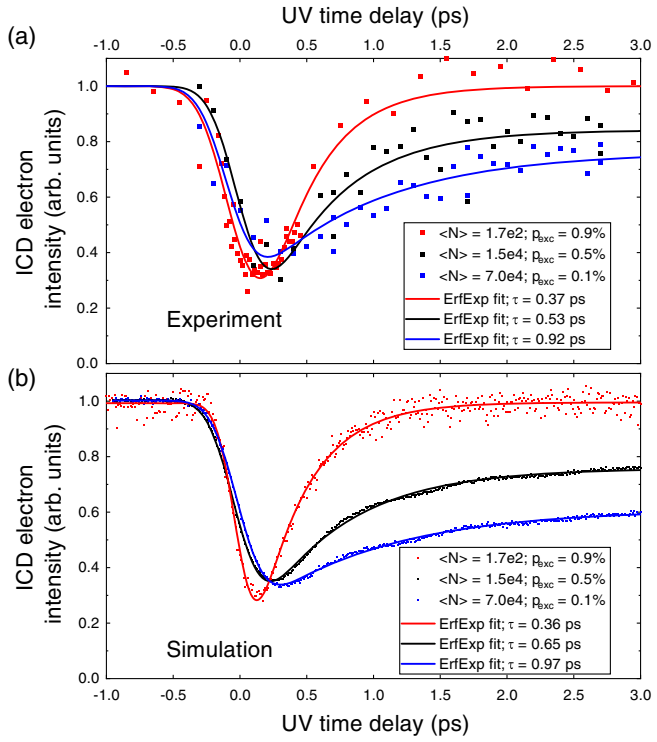

FIG. 7. (a) Experimental ICD electron intensities as a function of XUV-UV pump-probe delay with corresponding exponential fits for three different droplet sizes and excitation densities. (b) Simulated ICD electron intensities and fits for conditions similar to those of the upper panel.

shows that our model captures the main aspects of the pump-probe ICD dynamics.

APPENDIX D: THE EFFECT OF ATOMIC MOBILITY ON ICD TIMESCALES

Besides providing a deeper understanding of our experimental findings, MC simulations additionally allow us to ask more fundamental questions about the process, which cannot be directly addressed through experiment. For instance, how important is the mobility of the He^* atoms in the ICD process? To benchmark our simulations against a model system where the ICD rate is entirely given by the initial distances between He^*, we carry out simulations where the He^* positions are held fixed. Figure 8(a) shows the simulated ICD electron intensity for stationary He^* atoms as a function of the UV time delay for three different excitation probabilities (blue lines). For comparison, the experimental data are shown as black squares, and the corresponding MC simulation assuming mobile He^* atoms is shown as a red line. As can be clearly seen, the simulated dynamics for fixed He^* positions proceed on much longer timescales compared to the experimental data, thus showing the critical importance of atomic mobility in the ICD process. To further illustrate this point, Fig. 8(b) shows the relative

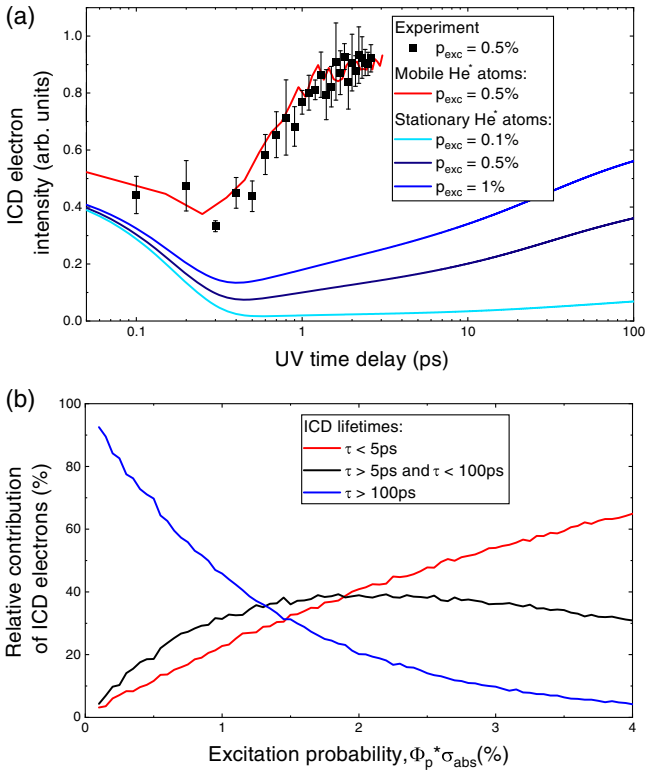

FIG. 8. (a) Simulated ICD electron intensities as a function of the UV time delay for fixed He* positions with different excitation densities (blue curves). For comparison, the experimental data are shown as black squares, and the corresponding MC simulation assuming mobile He* atoms is shown as a red line. (b) Relative contribution of ICD electrons broken up into three different ICD lifetime intervals as a function of excitation probability for fixed He* positions.

contribution of ICD electrons broken up into three different ICD lifetime intervals as a function of excitation probability for fixed He* positions. For low excitation probability ($\lesssim$1%), the ICD lifetime would primarily be $\tau > 100$ ps, which is dramatically longer than what is shown in Fig. 2 for similar experimental conditions. Only for high excitation probability ($\gtrsim$2%) do shorter ICD lifetimes ($\tau < 5$ ps) significantly contribute. We note that at 2.5% excitation probability the transition from ICD to CAI occurs, in agreement with previous findings [18].

[1] H. Wabnitz, L. Bittner, A. De Castro, R. Döhrmann, P. Gürtler, T. Laarmann, W. Laasch, J. Schulz, A. Swiderski, K. von Haeften *et al.*, *Multiple Ionization of Atom Clusters by Intense Soft X-Rays from a Free-Electron Laser*, Nature (London) **420**, 482 (2002).

[2] C. Bostedt, H. Thomas, M. Hoener, E. Eremina, T. Fennel, K.-H. Meiwes-Broer, H. Wabnitz, M. Kuhlmann, E. Plönjes, K. Tiedtke *et al.*, *Multistep Ionization of Argon Clusters in Intense Femtosecond Extreme Ultraviolet Pulses*, Phys. Rev. Lett. **100**, 133401 (2008).

[3] C. Bostedt, H. Thomas, M. Hoener, T. Möller, U. Saalmann, I. Georgescu, C. Gnodtke, and J.-M. Rost, *Fast Electrons from Multi-electron Dynamics in Xenon Clusters Induced by Inner-Shell Ionization*, New J. Phys. **12**, 083004 (2010).

[4] L. S. Cederbaum, J. Zobeley, and F. Tarantelli, *Giant Intermolecular Decay and Fragmentation of Clusters*, Phys. Rev. Lett. **79**, 4778 (1997).

[5] U. Hergenhahn, *Interatomic and Intermolecular Coulombic Decay: The Early Years*, J. Electron Spectrosc. Relat. Phenom. **184**, 78 (2011).

[6] T. Jahnke, *Interatomic and Intermolecular Coulombic Decay: The Coming of Age Story*, J. Phys. B **48**, 082001 (2015).

[7] T. Jahnke, U. Hergenhahn, B. Winter, R. Dörner, U. Frühling, P. V. Demekhin, K. Gokhberg, L. S. Cederbaum, A. Ehresmann, A. Knie *et al.*, *Interatomic and Intermolecular Coulombic Decay*, Chem. Rev. **120**, 11295 (2020).

[8] K. Gokhberg, P. Kolorenč, A. I. Kuleff, and L. S. Cederbaum, *Site- and Energy-Selective Slow-Electron Production through Intermolecular Coulombic Decay*, Nature (London) **505**, 661 (2014).

[9] F. Trinter, M. Schöffler, H.-K. Kim, F. Sturm, K. Cole, N. Neumann, A. Vredenborg, J. Williams, I. Bocharova, R. Guillemin *et al.*, *Resonant Auger Decay Driving Intermolecular Coulombic Decay in Molecular Dimers*, Nature (London) **505**, 664 (2014).

[10] V. Stumpf, K. Gokhberg, and L. S. Cederbaum, *The Role of Metal Ions in X-Ray-Induced Photochemistry*, Nat. Chem. **8**, 237 (2016).

[11] X. Ren, E. Wang, A. D. Skitnevskaya, A. B. Trofimov, K. Gokhberg, and A. Dorn, *Experimental Evidence for Ultrafast Intermolecular Relaxation Processes in Hydrated Biomolecules*, Nat. Phys. **14**, 1062 (2018).

[12] E. Allaria, R. Appio, L. Badano, W. A. Barletta, S. Bassanese, S. G. Biedron, A. Borga, E. Busetto, D. Castronovo, and P. e. a. Cinquegrana, *Highly Coherent and Stable Pulses from the Fermi Seeded Free-Electron Laser in the Extreme Ultraviolet*, Nat. Photonics **6**, 699 (2012).

[13] E. Allaria, A. Battistoni, F. Bencivenga, R. Borghes, C. Callegari, F. Capotondi, D. Castronovo, P. Cinquegrana, D. Cocco, M. Coreno *et al.*, *Tunability Experiments at the FERMI@Elettra Free-Electron Laser*, New J. Phys. **14**, 113009 (2012).

[14] A. I. Kuleff, K. Gokhberg, S. Kopelke, and L. S. Cederbaum, *Ultrafast Interatomic Electronic Decay in Multiply Excited Clusters*, Phys. Rev. Lett. **105**, 043004 (2010).

[15] A. LaForge, M. Drabbels, N. B. Brauer, M. Coreno, M. Devetta, M. Di Fraia, P. Finetti, C. Grazioli, R. Katzy, V. Lyamayev *et al.*, *Collective Autoionization in Multiply-Excited Systems: A Novel Ionization Process Observed in Helium Nanodroplets*, Sci. Rep. **4**, 3621 (2014).

[16] Y. Ovcharenko, V. Lyamayev, R. Katzy, M. Devetta, A. LaForge, P. O'Keeffe, O. Plekan, P. Finetti, M. Di Fraia, M. Mudrich *et al.*, *Novel Collective Autoionization Process Observed in Electron Spectra of He Clusters*, Phys. Rev. Lett. **112**, 073401 (2014).

[17] D. Iablonskyi, K. Nagaya, H. Fukuzawa, K. Motomura, Y. Kumagai, S. Mondal, T. Tachibana, T. Takanashi, T. Nishiyama, K. Matsunami *et al.*, *Slow Interatomic*

Coulombic Decay of Multiply Excited Neon Clusters, Phys. Rev. Lett. **117**, 276806 (2016).

[18] Y. Ovcharenko, A. C. LaForge, B. Langbehn, O. Plekan, R. Cucini, P. Finetti, P. O'Keeffe, D. Iablonskyi, T. Nishiyama, K. Ueda, P. Piseri, M. D. Fraia, R. Richter, M. Coreno, C. Callegari, K. C. Prince, F. Stienkemeier, T. Möller, and M. Mudrich, *Autoionization Dynamics of Helium Nanodroplets Resonantly Excited by Intense XUV Laser Pulses*, New J. Phys. **22**, 083043 (2020).

[19] K. Schnorr, A. Senftleben, M. Kurka, A. Rudenko, L. Foucar, G. Schmid, A. Broska, T. Pfeifer, K. Meyer, D. Anielski *et al.*, *Time-Resolved Measurement of Interatomic Coulombic Decay in* Ne_2, Phys. Rev. Lett. **111**, 093402 (2013).

[20] T. Takanashi, N. V. Golubev, C. Callegari, H. Fukuzawa, K. Motomura, D. Iablonskyi, Y. Kumagai, S. Mondal, T. Tachibana, K. Nagaya *et al.*, *Time-Resolved Measurement of Interatomic Coulombic Decay Induced by Two-Photon Double Excitation of* Ne_2, Phys. Rev. Lett. **118**, 033202 (2017).

[21] J. P. Toennies and A. F. Vilesov, *Superfluid Helium Droplets: A Uniquely Cold Nanomatrix for Molecules and Molecular Complexes*, Angew. Chem., Int. Ed. **43**, 2622 (2004).

[22] M. Shcherbinin, A. C. LaForge, V. Sharma, M. Devetta, R. Richter, R. Moshammer, T. Pfeifer, and M. Mudrich, *Interatomic Coulombic Decay in Helium Nanodroplets*, Phys. Rev. A **96**, 013407 (2017).

[23] F. Wiegandt, F. Trinter, K. Henrichs, D. Metz, M. Pitzer, M. Waitz, E. Jabbour Al Maalouf, C. Janke, J. Rist, N. Wechselberger *et al.*, *Direct Observation of Interatomic Coulombic Decay and Subsequent Ion-Atom Scattering in Helium Nanodroplets*, Phys. Rev. A **100**, 022707 (2019).

[24] D. Buchta, S. R. Krishnan, N. B. Brauer, M. Drabbels, P. O'Keeffe, M. Devetta, M. Di Fraia, C. Callegari, R. Richter, M. Coreno *et al.*, *Charge Transfer and Penning Ionization of Dopants in or on Helium Nanodroplets Exposed to EUV Radiation*, J. Phys. Chem. A **117**, 4394 (2013).

[25] R. Katzy, A. LaForge, Y. Ovcharenko, M. Coreno, M. Devetta, M. Di Fraia, M. Drabbels, P. Finetti, V. Lyamayev, T. Mazza *et al.*, *Migration of Surface Excitations in Highly-Excited Nanosystems Probed by Intense Resonant XUV Radiation*, J. Phys. B **48**, 244011 (2015).

[26] A. C. LaForge, V. Stumpf, K. Gokhberg, J. von Vangerow, F. Stienkemeier, N. V. Kryzhevoi, P. O'Keeffe, A. Ciavardini, S. R. Krishnan, M. Coreno *et al.*, *Enhanced Ionization of Embedded Clusters by Electron-Transfer-Mediated Decay in Helium Nanodroplets*, Phys. Rev. Lett. **116**, 203001 (2016).

[27] A. LaForge, M. Shcherbinin, F. Stienkemeier, R. Richter, R. Moshammer, T. Pfeifer, and M. Mudrich, *Highly Efficient Double Ionization of Mixed Alkali Dimers by Intermolecular Coulombic Decay*, Nat. Phys. **15**, 247 (2019).

[28] L. Ben Ltaief, M. Shcherbinin, S. Mandal, S. Krishnan, A. LaForge, R. Richter, S. Turchini, N. Zema, T. Pfeifer, E. Fasshauer *et al.*, *Charge Exchange Dominates Long-Range Interatomic Coulombic Decay of Excited Metal-Doped Helium Nanodroplets*, J. Phys. Chem. Lett. **10**, 6904 (2019).

[29] L. B. Ltaief, M. Shcherbinin, S. Mandal, S. R. Krishnan, R. Richter, T. Pfeifer, M. Bauer, A. Ghosh, M. Mudrich, K. Gokhberg *et al.*, *Electron Transfer Mediated Decay of Alkali Dimers Attached to He Nanodroplets*, Phys. Chem. Chem. Phys. **22**, 8557 (2020).

[30] K. von Haeften, T. Laarmann, H. Wabnitz, and T. Möller, *Bubble Formation and Decay in* ^{3}He *and* ^{4}He *Clusters*, Phys. Rev. Lett. **88**, 233401 (2002).

[31] M. Mudrich, A. LaForge, A. Ciavardini, P. OKeeffe, C. Callegari, M. Coreno, A. Demidovich, M. Devetta, M. Di Fraia, M. Drabbels *et al.*, *Ultrafast Relaxation of Photoexcited Superfluid He Nanodroplets*, Nat. Commun. **11**, 112 (2020).

[32] H.-B. Zhou, J.-L. Wang, W. Jiang, G.-H. Lu, J. Aguiar, and F. Liu, *Electrophobic Interaction Induced Impurity Clustering in Metals*, Acta Mater. **119**, 1 (2016).

[33] D. Chandler, *Interfaces and the Driving Force of Hydrophobic Assembly*, Nature (London) **437**, 640 (2005).

[34] M. Joppien, R. Karnbach, and T. Möller, *Electronic Excitations in Liquid Helium: The Evolution from Small Clusters to Large Droplets*, Phys. Rev. Lett. **71**, 2654 (1993).

[35] M. Barranco, R. Guardiola, S. Hernández, R. Mayol, J. Navarro, and M. Pi, *Helium Nanodroplets: An Overview*, J. Low Temp. Phys. **142**, 1 (2006).

[36] F. Ancilotto, M. Barranco, F. Coppens, J. Eloranta, N. Halberstadt, A. Hernando, D. Mateo, and M. Pi, *Density Functional Theory of Doped Superfluid Liquid Helium and Nanodroplets*, Int. Rev. Phys. Chem. **36**, 621 (2017).

[37] V. Lyamayev, Y. Ovcharenko, R. Katzy, M. Devetta, L. Bruder, A. LaForge, M. Mudrich, U. Person, F. Stienkemeier, M. Krikunova *et al.*, *A Modular End-Station for Atomic, Molecular, and Cluster Science at the Low Density Matter Beamline of FERMI@Elettra*, J. Phys. B **46**, 164007 (2013).

[38] D. Verma and A. F. Vilesov, *Pulsed Helium Droplet Beams*, Chem. Phys. Lett. **694**, 129 (2018).

[39] B. Dick, *Inverting Ion Images without Abel Inversion: Maximum Entropy Reconstruction of Velocity Maps*, Phys. Chem. Chem. Phys. **16**, 570 (2014).

[40] T. N. Chang and T. K. Fang, *Effect of Positive-Energy Orbitals on the Photoionization Cross Sections and Oscillator Strengths of He and Divalent Atoms*, Phys. Rev. A **52**, 2638 (1995).

[41] See Supplemental Material at http://link.aps.org/supplemental/10.1103/PhysRevX.11.021011 for additional details on the theoretical calculations and modeling.

[42] T. Miteva, S. Kazandjian, and N. Sisourat, *On the Computations of Decay Widths of Fano Resonances*, Chem. Phys. **482**, 208 (2017).

[43] D. Scharf, J. Jortner, and U. Landman, *Vibrational Predissociation Induced by Exciton Trapping in Inert-Gas Clusters*, Chem. Phys. Lett. **126**, 495 (1986).

[44] A. Scheidemann, B. Schilling, and J. P. Toennies, *Anomalies in the Reactions of Helium (1+) with Sulfur Hexafluoride Embedded in Large Helium-4 Clusters*, J. Phys. Chem. **97**, 2128 (1993).

[45] K. D. Closser, O. Gessner, and M. Head-Gordon, *Simulations of the Dissociation of Small Helium Clusters with Ab Initio Molecular Dynamics in Electronically Excited States*, J. Chem. Phys. **140**, 134306 (2014).

[46] J. Seong, K. C. Janda, N. Halberstadt, and F. Spiegelmann, *Short-Time Charge Motion in* He_n^+ *Clusters*, J. Chem. Phys. **109**, 10873 (1998).

[47] A. Hernando, M. Barranco, M. Pi, E. Loginov, M. Langlet, and M. Drabbels, *Desorption of Alkali Atoms from* ^{4}He *Nanodroplets*, Phys. Chem. Chem. Phys. **14**, 3996 (2012).

[48] H. Buchenau, J. P. Toennies, and J. A. Northby, *Excitation and Ionization of* ^{4}He *Clusters by Electrons*, J. Chem. Phys. **95**, 8134 (1991).

[49] B. Thaler, S. Ranftl, P. Heim, S. Cesnik, L. Treiber, R. Meyer, A. W. Hauser, W. E. Ernst, and M. Koch, *Femtosecond Photoexcitation Dynamics inside a Quantum Solvent*, Nat. Commun. **9**, 4006 (2018).

[50] K. von Haeften, T. Laarmann, H. Wabnitz, T. Möller, and K. Fink, *Size and Isotope Effects of Helium Clusters and Droplets: Identification of Surface and Bulk-Volume Excitations*, J. Phys. Chem. A **115**, 7316 (2011).

[51] P. Nijjar, A. Krylov, O. Prezhdo, A. Vilesov, and C. Wittig, *Conversion of* $He(2^3s)$ *to* He_2 $(a^3\sigma_u^+)$ *in Liquid Helium*, J. Phys. Chem. Lett. **9**, 6017 (2018).

[52] T. Möller, K. von Haeften, T. Laarman, and R. von Pietrowski, *Photochemistry in Rare Gas Clusters*, Eur. Phys. J. D **9**, 5 (1999).

[53] I. Unger, R. Seidel, S. Thürmer, M. N. Pohl, E. F. Aziz, L. S. Cederbaum, E. Muchová, P. Slavíček, B. Winter, and N. V. Kryzhevoi, *Observation of Electron-Transfer-Mediated Decay in Aqueous Solution*, Nat. Chem. **9**, 708 (2017).

[54] M. Gramlich, B. J. Bohn, Y. Tong, L. Polavarapu, J. Feldmann, and A. S. Urban, *Thickness-Dependence of Exciton-Exciton Annihilation in Halide Perovskite Nanoplatelets*, J. Phys. Chem. Lett. **11**, 5361 (2020).

[55] B. J. Walker, A. J. Musser, D. Beljonne, and R. H. Friend, *Singlet Exciton Fission in Solution*, Nat. Chem. **5**, 1019 (2013).

[56] G. Jones and D. Bradshaw, *Resonance Energy Transfer: From Fundamental Theory to Recent Applications*, Front. Phys. **7**, 100 (2019).

[57] M. P. Ziemkiewicz, D. M. Neumark, and O. Gessner, *Ultrafast Electronic Dynamics in Helium Nanodroplets*, Int. Rev. Phys. Chem. **34**, 239 (2015).

[58] E. Fasshauer and L. B. Madsen, *Time-Resolved Spectroscopy of Interparticle Coulombic Decay Processes*, Phys. Rev. A **101**, 043414 (2020).